Materials Today Advances 29 (2026) 100686

Contents lists available at ScienceDirect

Materials Today Advances

journal homepage: www.journals.elsevier.com/materials-today-advances/

Photo-crosslinked networks based on panthenol-derived polyesters: degradable materials for biomedical applications

Isabela Lima Autran Dourado [a], Daniel Franco Minatelli [a], Anna Szabó [b], Denisse Esther Mallaupoma Camarena [a], Flávia Gonçalves [c], Sandra Van Vlierberghe [b], Luiz Henrique Catalani [a,*]

[a] Departamento de Química Fundamental, Instituto de Química, Universidade de São Paulo, São Paulo, SP, 05508-000, Brazil
[b] Polymer Chemistry and Biomaterials Group, Centre of Macromolecular Chemistry, Department of Organic and Macromolecular Chemistry, Ghent University, Krijgslaan 281 S4, 9000, Ghent, Belgium
[c] Departamento de Odontologia, Universidade de Santo Amaro, São Paulo, SP, 04829-300, Brazil

ARTICLE INFO

Keywords:
Panthenol
Panthenyl-polymers
Photo-crosslinking
Vinylic monomers
Degradable biomaterial
Tissue engineering

ABSTRACT

Tissue engineering has an increasing demand for safe materials that can support complex architectures in tissue regeneration. The development of new biodegradable polymers is a challenge that needs to be constantly addressed to drive the advancements towards biomedical applications. In this study, a new polyester based on D, L-panthenol, poly(D,L-4,3′-panthenyl adipate) (PPA), was successfully synthesized, modified, and photo-crosslinked. While panthenol (also called provitamin B5, a cofactor present in a plethora of metabolic reactions) is widely used in the cosmetic industry due to its moisturizing and wound-healing properties, to the best of our knowledge, no previous records of panthenol-derived polycondensation exist in the literature. The synthesized PPA, a polyol, was modified by introducing acryloyl moieties, yielding an amorphous PPA acrylate with around 67 % of double bonds. The acrylate system allows the incorporation of a wide range of co-crosslinkers with diverse reactivities and functional groups, enabling straightforward tuning of network properties. Various co-monomers or co-crosslinkers were incorporated, including N-isopropylacrylamide, N-vinylpyrrolidone, 1-vinylimidazole, 1,6-hexanediol diacrylate, and divinyl adipate, yielding exceptional efficiency in photo-curing, achieving high network densities with rapid gelation kinetics, and full double bond conversion. The systems have proven to be hydrolytically degradable with tunable degradation rates and non-cytotoxic towards NIH-3T3 cell lines. These photo-curable systems are promising candidates for light-based scaffold biofabrication techniques. Moreover, the potential for panthenol-derived polymer functionalization with different unsaturated groups unlocks exciting possibilities for biomedical applications.

1. Introduction

Alongside the increase in life expectancy, the demand for innovative solutions addressing organ repair, failure, and transplantation has driven the development of novel biomaterials and advanced processes for medical device fabrication [1]. In the context of implants, the ideal material combines appropriate chemical nature with a rational design to achieve the physicochemical, biological, and mechanical properties specific to the target-tissue. In the field of Tissue Engineering (TE), such implants are often scaffolds, that is, devices that support tissue regeneration by permitting mass transport while simultaneously providing mechanical support for cellular adhesion, proliferation, and differentiation.

TE is a domain that employs various methods for scaffold fabrication, including solvent casting, gas foaming, freeze-drying, salt leaching, electrospinning, molding, and advanced additive manufacturing techniques [2,3]. Despite rapid advancements in bioengineering technologies, the development of biodegradable biomaterials tailored to meet the specific requirements of target tissues remains a persistent challenge, given the intricate nature of biological tissues. The availability of photosensitive materials for light-based biofabrication techniques (such as 2D micropatterning, photo-curable coatings and films, *in situ* photo-crosslinking of injectable systems, dynamic biomaterials and mainly stereolithography-based 3D printing technologies) is diverse.

* Corresponding author.
E-mail address: catalani@usp.br (L.H. Catalani).

https://doi.org/10.1016/j.mtadv.2026.100686
Received 22 April 2025; Received in revised form 14 September 2025; Accepted 31 December 2025

However, it remains extremely limited in terms of materials that are both biocompatible and biodegradable, creating a notable challenge in advancing applications for tissue engineering and related biomedical fields.

Photo-curable formulations typically consist of a polymer containing polymerizable moieties and a photo-initiator with the possible inclusion of solvent and other additives [4]. It is essential that all components exhibit minimal toxicity after processing (following crosslinking) and enable the material to degrade within a time span compatible with the regeneration of the target-tissue. In this work, we propose novel photo-curable formulations constituted by an unprecedented panthenol-derived polyester and different co-monomers and co-crosslinkers. The use of different vinylic monomers in the photocurable formulations endowed the studied materials with a feature essential for Tissue Engineering applications: the potential for fine customization of scaffolds to achieve chemical, physical, and biological properties tailorable to different target-tissues.

Panthenol, as known as pantothenol, panthothenyl alcohol, 2,4-dihydroxy-N-(3-hydroxypropyl)-3,3-dimethylbutanamide or provitamin B5, is the precursor of pantothenic acid (vitamin B5). This acid is a component of coenzyme A, a cofactor of utmost importance in lipid biosynthesis, gluconeogenesis, tricarboxylic acid cycle, cholesterol, steroid hormones, vitamin A, vitamin D, and porphyrin metabolisms [5,6]. Pantothenate is also required in the synthesis of amino acids such as leucine, arginine, and methionine [5]. Panthenol is widely used in cosmetics and hair products [7–9] due to its hygroscopic nature and essential role in addressing skin disorders. It exhibits anti-inflammatory activity and promotes fibroblast proliferation and epidermal reepithelialization [6]. The compound is soluble in water and alcohol and has physical properties suitable for formulating many pharmaceutical dosage forms, such as gels, creams, ointments, and hydrogels. These attributes further underscore its potential as a versatile ingredient in sunscreens, hydrating creams, and multivitamin supplements.

Intriguingly, despite the impressive array of panthenol applications and to the best of our knowledge, the literature lacks reports of its direct polymerization. Kabir and co-workers [10] have described a method for producing the first pantothenic acid derivative monomer (B5AMA) by reacting D-pantolactone with 2-aminoethyl methacrylamide (by ring opening chemistry). Then, B5AMA, an unsaturated compound, was chemically crosslinked in the presence of N′,N′-methylene bisacrylamide, yielding an extremely hygroscopic hydrogel with antifouling properties.

Although rarely reported, panthenol esterification has already been investigated [11–15]. The selective synthesis of monoester panthenol derivatives via traditional protocols that requires protection/deprotection steps gives modest yields [11]. Panthenyl triacetate with yields up to 80 % can be produced by reacting panthenol with acetic anhydride using a heterogenous catalyst based on dimethylaminopyridine [12]. Diego and co-authors [13] have shown for the first time a method to produce regioselective mono- and di-panthenyl-esters using immobilized *Candida antarctica* lipase B (Novozym 435) as the catalyst. Nieto and co-workers [14] have shown the selective production of mono-acyl esters under solvent-free conditions using Novozym 435 (the tri-acyl ester was never detected). The enzymatic synthesis of panthenyl monoacyl esters was also reported with high conversion and selectivity by using ionic liquids [15].

Lipases are one of the most extensively used enzymes in biocatalysis. In an excellent review, Ortiz and co-workers [16] affirm that they are stable in different media, like ionic liquids, organic solvents, aqueous media, and supercritical fluids. Besides that, these enzymes are used not only as hydrolases (natural function), but also in esterification, transesterification, aminolysis, and perhydrolysis reactions [16]. CAL-B is the main lipase used, with its structure being fully elucidated [17] and its catalytic mechanism being well-known [18]. The enzyme is available physically immobilized in Lewatit VP OC 1600, a macroporous acrylic polymer, via interfacial activation [19]. In the literature, immobilized CAL-B have already shown a high regioselectivity for the primary hydroxyl groups from panthenol [13]. Despite the fact that CAL-B can catalyze esterification and transesterification reactions, it usually does so by reaction with primary hydroxyl groups. The reaction with secondary diols is possible with very slow kinetics, under highly specific conditions [20–22].

Herein, for the first time, poly(D,L-4,3′-panthenyl adipate), PPA, was synthesized via polycondensation between D,L-panthenol and diethyl adipate catalyzed by Novozym 435. The polyol PPA, a saturated macromolecule, is not a photo-curable polymer, so a modification with acrylic moieties was carried out, yielding PPA acrylate (PPA-AC). Although PPA-AC was proven to be photo-curable by itself, the polymer was also combined with different co-monomers and co-crosslinkers (N-isopropylacrylamide, N-vinylpyrrolidone, 1-vinylimidazole, 1,6-hexanediol diacrylate, and divinyl adipate) selected due their high reactivity in free-radical polymerization, differences in their hydrophilic/hydrophobic nature and their demonstrated biocompatibility in analogous systems. Also, these unsaturated compounds were chosen based on their successful performance in our previous study (https://doi.org/10.1039/d5py00237k).

The formulations allowed the development of networks with varying viscoelastic and mechanical properties, hydrolytic degradation kinetics, and cellular response, while ensuring full double bond conversion. Rather than focusing on a single target tissue, our aim was to develop versatile systems: these different photo-curable formulations can be adapted for a variety of biomedical purposes, thereby expanding the toolbox of materials available for medical applications.

2. Experimental section

2.1. Materials

All solvents (Sigma Aldrich, USA) were purified and dried before use. Diethyl adipate (Sigma Aldrich, USA) was distilled under reduced pressure prior to its use. D,L-Panthenol (Sigma Aldrich, USA) was recrystallized from acetone and dried under vacuum at 50 °C until constant mass. Novozym 435 (NZ 435, specific activity of 10,500 PLU/g) was kindly donated by Novozymes Latin America Ltda (Brazil) and consists of *Candida antarctica* lipase B (CAL-B) adsorbed within the macroporous resin Lewatit VPOC 1600 poly[methyl methacrylate-*co*-butyl methacrylate]). Acryloyl chloride (Merck, Germany) was used as received. Triethylamine (Sigma Aldrich, USA) was dried over calcium hydride (Sigma Aldrich, USA) and then distilled. Ammonium chloride and magnesium sulfate (both from Anidrol, Brazil) were used as received. N-isopropylacrylamide (Sigma Aldrich, USA) was recrystallized twice from a toluene/hexane (60:40) mixture and dried under vacuum at 40 °C. N-vinylpyrrolidone and N-vinylimidazole (Sigma Aldrich, USA) were distilled under reduced pressure. 1,6-hexanediol diacrylate (Sigma Aldrich, USA), bis(2,4,6-trimethylbenzoyl)-phenylphosphineoxide (BAPO, Sigma Aldrich, USA), and ethyl(2,4,6-trimethylbenzoyl) phenyl phosphinate (TPO-L, Lambson Ltd HQ, UK) were used as received. Ultrapure water was obtained using a Milli-Q system.

2.2. Methods

The methods described in this study to produce polymers based on panthenol contemplate the following reactions (Scheme 1).

2.2.1. Enzymatic synthesis of poly(D,L-4,3′-panthenyl adipate)

Polycondensation reactions of D,L-panthenol (4.10 g, 20 mmol) and diethyl adipate (4.10 g, 20 mmol) were carried out using Novozym 435 (10 % w/w) as catalyst and cyclohexane as solvent (Scheme 1). The reactants were added to a 250 mL round-bottom flask containing 150 mL of solvent. A Dean-Stark apparatus, loaded with 10 g of 4 Å molecular sieves on the collector chamber, was attached to the flask, along with a

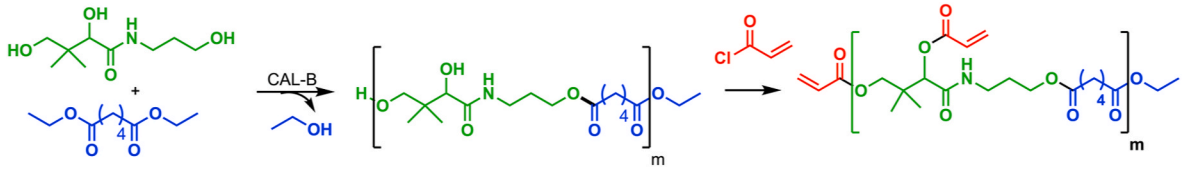

Scheme 1. Schematic representation of the enzymatic polycondensation reaction between panthenol and diethyl adipate followed by acrylation of PPA, yielding PPA-AC.

condenser. The reaction mixture was magnetically stirred and refluxed using an oil bath at 90 °C. The setup was covered with aluminum foil to retain heat. After 16 h of reaction, the final mixture was dissolved in chloroform and filtered to remove the enzyme. The solvent was removed by rotary-evaporation, and the resulting oligomers were dissolved in a minimal amount of chloroform and, subsequently, dropwise added in diethyl ether (10 times the chloroform volume). The supernatant was removed and the precipitated product was carefully concentrated and dried under vacuum for 72 h, yielding poly(D,L-4,3′-panthenyl adipate), hereinafter referred to as poly(panthenyl adipate) or PPA, a colorless and viscous product.

2.2.2. Poly(panthenyl adipate) acrylation

Several different acrylation protocols can be found in literature [23–26]. Herein, PPA (4.62 g) was dissolved in 50 mL of CH_2Cl_2 in a 250 mL round-bottom flask, followed by addition of triethylamine (2.98 mL, 0.021 mol) under vigorous stirring. The reaction mixture was cooled to 0 °C and acryloyl chloride (1.51 mL, 0.019 mol) dissolved in 20 mL of CH_2Cl_2 was added via a dropping funnel (Scheme 1). The system was kept under nitrogen atmosphere and protected from light. After 16 h of reaction, the solution was three times washed with 50 mL of saturated ammonium chloride solution. Organic phases were combined, and the solution was dried by adding anhydrous magnesium sulfate, followed by filtration and subsequent removal of the solvent. The polymer was dissolved in a minimal amount of chloroform and dropwise added to cold diethyl ether. The final product, poly(panthenyl adipate) acrylate (PPA-AC), was concentrated by rotary evaporation and then dried under vacuum for 72 h.

2.2.3. Photo-crosslinking studies

Photo-crosslinking reactions were carried out by irradiation of formulations prepared as follows: solutions of polymer (PPA-AC, 250 mg), photo-initiator (BAPO, 14 mg) and different co-monomers or co-crosslinkers (Fig. 1) were dissolved in 550 μL of dichloroethane. This mixture was homogenized using a vortex. After homogenization, formulations were added to open cylindrical Teflon® molds and photo-crosslinked using a BioLambda® LED box (chamber dimensions of 141 x 43 × 116 mm^3, wavelength of 410 nm and 27 mW cm^{-2} of radiance measured by means of a dosimeter). The samples were exposed to light for 30 s, 1 min versus 5 min.

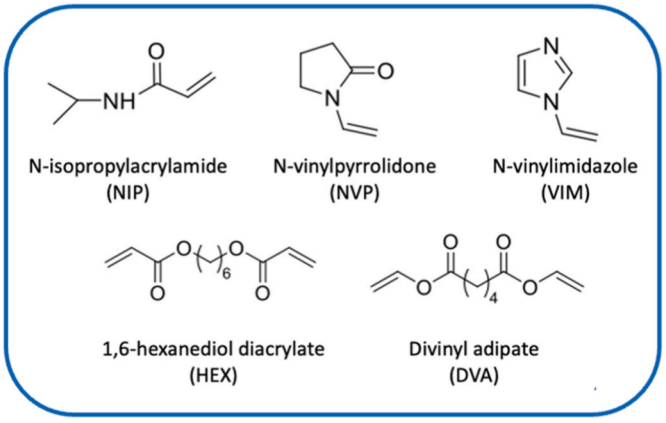

Fig. 1. Structures of co-monomers and co-crosslinkers used.

N-isopropylacrylamide (NIP), N-vinylimidazole (VIM), N-vinylpyrrolidone (NVP), 1,6-hexanediol-diacrylate (HEX), and divinyl adipate (DVA) were used as co-monomers or co-crosslinkers (Fig. 1). Formulations were also produced without co-crosslinkers by mixing only the polymer, solvent and photo-initiator. The amount of co-crosslinker used depended on whether it contained one (NIP, VIM, NVP) or two (HEX, DVA) vinylic groups. For co-monomers with a single vinylic group, 1.06 mmol was used, while 0.53 mmol was used for those with two vinylic groups (co-crosslinkers), ensuring that all formulations had an equivalent concentration of reactive double bonds. While PPA-AC can be effectively photo-crosslinked without co-monomers or co-crosslinkers, the incorporation of these reactive additives was expected to substantially modify the networks' properties.

2.2.4. Polymer characterization

Size Exclusion Chromatography (SEC) was used to evaluate $\overline{M_n}$, $\overline{M_w}$ and polydispersity index on a Malvern Instruments, Viscotel 305 TDA Chromatograph, triple detection (refraction index at 35 °C, light scattering and viscometer), loop of 200 μL, pump VE 2001. The mobile phase was THF at a flow rate of 1 mL min^{-1}. The system was set up with a pre-column and three Viscotek columns set up in series: T600 M (General Mixed Org, 300 × 8 mm, exclusion limit of de 20,000,000 g mol^{-1}), I-MBMMW 3078 (300 × 8 mm, exclusion limit of 200,000 g mol^{-1}), and I-Oligo 3078 (300 × 8 mm, exclusion limit of 10,000 g mol^{-1}). This set of columns is effective for low molecular weight polymers. The system was calibrated using a series of low polydispersity polystyrene standards (Aldrich/Waters, 820, 1200, 2,460, 4,300, 13,200, 29,300, 47,500, 216,000 and 1,210,000 g mol^{-1}). Toluene was used to determine the exclusion limit (standard calibration). 100 μL of 10 mg mL^{-1} polymer solutions were injected.

Nuclear Magnetic Resonance Spectroscopy (NMR). ^{1}H NMR analyses were executed on a Bruker AIII500 spectrometer (500 MHz). Polymer samples (10–15 mg) were solubilized in 650 μL of $CDCl_3$ containing TMS as internal reference.

Thermal Gravimetric Analysis (TGA) was performed to determine the degradation temperature of the synthesized panthenol-derived polyesters. The experiments were performed in a TA instruments TGA Q500. Each sample, weighing 5 mg, was placed in a Pt crucible and analyzed under nitrogen atmosphere, applying a heating rate of 10 °C min^{-1} from 0° to 700 °C.

Differential Scanning Calorimetry (DSC) analyses were performed on a TA Instruments Q20 calorimeter. Samples weighing 8 mg were placed in Al pans and analyzed under nitrogen flow. The thermal cycle involved an initial heating from −70 °C to 110 °C, followed by cooling from 110 °C to −70 °C, and a subsequent second heating from −70 °C to 110 °C. Both the heating and cooling rates were set at 10 °C min^{-1}.

Matrix Assisted Laser Desorption Ionization – Time of Flight (MALDI-TOF) analyses were carried out in an MALDI-TOF/TOF UltrafleXtreme equipment connected to two detectors using a pulsed UV laser and an ion acceleration electric field of 20 kV. Solutions were prepared by mixing dithranol as matrix (10 mg mL^{-1}, 30 μL), NaI as cationic agent (5 mg mL^{-1}, 3 μL), and polymer samples (10 mg mL^{-1}, 10 μL). $CHCl_3$:THF (1:1 v/v) mixture was used to prepare all the solutions, and 0.5 μL of the final mixture was used.

2.2.5. Crosslinked films characterization

Photo-rheology. Photo-rheology experiments were performed to investigate changes in the material viscoelastic behavior during light exposure. An Anton Paar Physica MR 301 rheometer equipped with a light source (27.5 mW cm^{-2}, filter 400–500 nm) was used. Approximately 300 μL of each formulation was placed between two parallel plates (PP25 spindle - top plate diameter of 25 mm, bottom plate of quartz, gap of 0.300 mm). Measurements were performed with a frequency of 1 Hz and amplitude of 0.1 %, in triplicate at 23 °C. The samples were exposed to light after 60 s of stabilization, and then a normal force of 1 N was applied. The storage (G′) and the loss moduli (G″) were recorded during 2 min of light exposure to each photo-curable formulation.

Gel fraction and swelling degree studies. Photo-crosslinked sheets obtained after photo-crosslinking were removed from Teflon® molds and were dried in an oven at 40 °C for 48 h for solvent removal. Samples (approximately 50 mg in weight, about 0.5 mm of thickness) were weighed (W_i) and placed into 5 mL eppendorfs containing chloroform. After reaching swelling equilibrium (at least 24 h), films were removed from chloroform, blotted dry with filter paper, and then weighed (W_s). Finally, the samples were left drying under vacuum until constant mass (W_d). All measurements were carried out in triplicate.

The gel fraction (GF) and the equilibrium swelling ratio (or swelling degree, SD) were calculated, respectively, using the following equations:

$$GF_{(\%)} = \frac{W_d}{W_i}\, x\, 100\% \tag{1}$$

$$SD_{(\%)} = \frac{W_s - W_d}{W_d}\, x\, 100\% \tag{2}$$

It is worth mentioning that the swelling degree was also determined in ultrapure water, following the same equation (2).

FT-Raman Scattering Spectroscopy was performed in a Bruker RFS-100/S (Nd/YAG, λ = 1064 nm), a diode detector Ge refrigerated using liquid nitrogen. Measurements were acquired from 100 to 4000 cm^{-1}, with 4 cm^{-1} resolution and 32 accumulations. Laser potential varied from 100 to 300 mW, depending on the sample specific characteristics.

High Resolution Magic Angle Spinning Nuclear Magnetic Resonance Spectroscopy (HR-MAS ^{1}H-NMR) was performed using a BrukerUltrashield+ 500 MHz Avance II spectrometer and a triple channel HR-MAS probe head. A spinning frequency of 6000 Hz was applied, 32 scans of 64,000 points were collected. The spectrometer excitation frequency used was 4900.9 ppm. Measurements were carried out in deuterated chloroform at 25 °C.

Contact Angles and Surface Energy. The contact angle measurements were performed by the drop-sessile method in a goniometer (Tantec, CAM-PLUS micro), an apparatus that consists of a light source, an adjustable height support for the sample, a magnifying glass and a screen with different angles, on which the image of the drop is projected, and its angles can be measured. Glycerol, diiodomethane and ultrapure water were used as liquid-references.

The traditional spin-coating technique, typically used to produce flat films with minimal roughness, is not suitable for pre-curing solution photo-crosslinking. This is due to the evaporation of the solvents during the process, affecting the replication of a crosslinked film's surface. Consequently, an alternative method was devised to produce these samples as follows: 40 μL of the formulation was deposited onto a microscopy slide (Starfrost). A rectangular-cut silica plate was then placed over the slide. This assembly—comprising the slide, solution, and silica—was exposed to light for 5 min, with the glass side facing the light source. The system was left to dry for 4 h, after which the glass was carefully separated from the silica, leaving the flat photo-crosslinked film adhered to the glass slide alone. Subsequently, 10 μL of each solvent-reference was dripped onto the film, and the contact angle (θ) was measured. 5 μL was removed from the droplet to have the receding angle. All measurements performed here presented a hysteresis angle below 10°, suggesting a flat surface.

Surface tensions, polar and dispersive components were calculated as suggested by van Oss and co-authors [27], using equations (3) and (4):

$$\Upsilon_L(1+\cos\Theta) = 2\sqrt{\Upsilon_S^{LW}.\,\Upsilon_L^{LW}} + 2\sqrt{\Upsilon_S^{+}.\,\Upsilon_S^{-}} + 2\sqrt{\Upsilon_S^{-}.\,\Upsilon_L^{+}} \tag{3}$$

$$\Upsilon_S = \Upsilon_S^{LW} + 2\sqrt{\Upsilon_S^{+}.\Upsilon_S^{-}} \tag{4}$$

where Υ_S is the surface tension, which is divided into different perceived components: Υ^{LW}, Υ_S^{+} and Υ_S^{-}, representing, respectively, Liftshitz-van de Waals component (dispersive component), acid and basic components (polar components); S or L denotes a solid or a liquid phase. Surface tension parameters (mJ m^{-2}) from known solvents were used: ultrapure water (Υ_L = 72.8; Υ_L^{LW} = 21.8; Υ_L^{+} = 25.5; Υ_L^{-} = 25.5) [28], glycerol (Υ_L = 64; Υ_L^{LW} = 34; Υ_L^{+} = 3.9; Υ_L^{-} = 57.4) [28], and diiodomethane (Υ_L = 50.8; Υ_L^{LW} = 50.8; Υ_L^{+} = 0; Υ_L^{-} = 0) [28].

It is worth mentioning that an exposure time of 5 min was selected to simulate the condition of maximum photo-crosslinking, providing more reliable information about the surface characteristics of films. The aim was also to compare the surface properties of the films produced with different co-monomers or co-crosslinkers.

Dynamical-Mechanical Analysis. The films obtained in the "Photo-crosslinking Studies" section were cut into strips of 0.5 cm × 3 cm x 0.7 mm (width, length, thickness). In order to characterize the mechanical properties of a material when it is subjected to dynamic forces, a dynamic-mechanical analysis was carried out in an equipment from TA Instruments, model DMA Q800. Calibration was performed at 30 °C and ramp measurements were taken at a rate of 0.5 N min^{-1} up to 18 N. Stress measurements were performed by deformation of rectangular films (about 30 mm in length, 5 mm in width). Data were collected in triplicate for each sample.

Hydrolytic Degradation Assays. Discs with a diameter of 7 mm and thickness of 0.7 mm were cut from the films of PPA-AC with different co-monomers/co-crosslinkers and stored in a vacuum oven (Marconi, MA 030/12) at 50 °C until constant mass was achieved (48 h). Each sample was weighed and placed in 5 mL of a 0.05 M NaOH solution (accelerated conditions) or 5 mL of phosphate buffered solution (PBS, pH 7.8), both at 37 °C. At predetermined time points, the films were taken out from the solutions, extensively rinsed with ultrapure water, and dried in a vacuum oven at 50 °C until constant mass. The remaining mass was calculated. All degradation experiments were performed in triplicate.

2.2.6. In vitro cytotoxicity assays

2.2.6.1. Films preparation for cell culture assay. To prepare the films for the cytotoxicity assays, firstly, a gradual solvent exchange process was carried out to remove any potentially toxic residues and contaminants. The PPA-AC photo-crosslinked discs of 7 mm were immersed in chloroform for 48 h, with a solvent refreshment after the first 24 h. The same procedure was repeated using absolute ethanol. A final wash was performed in ultrapure water for 2 h. After the washing steps, the materials were dried in a vacuum oven for 48 h to eliminate any remaining solvent.

2.2.6.2. Cell culture. NIH-3T3 cells were cultured in Dulbecco's Modified Eagle Medium (DMEM) (Vitrocell, Embriolife, Brazil) supplemented with 10 % heat-inactivated fetal bovine serum (Vitrocell, Embriolife, Brazil) and maintained in an incubator at 37 °C with 5 % CO_2 until reaching 80 % confluence, at which point they were applied to the polymeric materials.

2.2.6.3. Cell counting and viability assessment by trypan blue exclusion. The photo-crosslinked films were evaluated in the form of discs

approximately 11 mm in diameter, with an average mass of 35 mg per disc. The discs were sterilized using UV-C irradiation for 20 min on each side. To ensure direct contact between the cells and the materials, each disc was placed in a 24-well plate and secured with supports to maintain stability at the bottom of the well. A total of 10^4 cells were seeded onto each disc and maintained in DMEM supplemented with 10 % fetal bovine serum (FBS) at 37 °C in a humidified atmosphere containing 5 % CO_2. Culture medium was replaced every 2 days. Cytotoxicity assessments were conducted after 3 and 7 days of incubation.

After exposure to the polymeric discs (during 3 and 7 days), cells were counted using a Neubauer chamber, and cell viability was determined by the Trypan Blue exclusion assay. For this, cells maintained in incubation were first washed with PBS, then treated with 0.25 % trypsin/EDTA solution (Vitrocell, Embriolife, Brazil) and incubated at 37 °C with 5 % CO_2. Trypsin was neutralized with DMEM containing 10 % FBS, and the cell suspension was centrifuged. After discarding the supernatant, cells were resuspended in 50 μL of DMEM. Then, 50 μL of a 0.4 % Trypan Blue solution was added to each cell suspension. After gently mixing, 10 μL of the mixture was loaded onto a Neubauer chamber for counting. Herein, "control" refers to cells grown on tissue-culture-treated polystyrene plates (TCPS).

Instead of representing the results as percentages of cell viability, we chose to present the total number of viable and non-viable cells counted. This approach allows not only the determination of relative viability but also the comparison of differences in absolute cell numbers.

Experiments were performed in duplicate using two polymer discs per material (N = 2). For each disc, cell counts were obtained in duplicate (n = 2). Results are reported as mean ± standard deviation.

3. Results and discussion

3.1. Synthesis and characterization of PPA and PPA-AC

In order to produce new photo-curable biocompatible formulations based on unprecedented panthenol-derived polymers, the following steps were carried out: (i) enzymatic synthesis of a saturated polyester based on panthenol – poly(D,L-4,3′-panthenyl adipate), PPA; (ii) modification with acrylate groups; and (iii) panthenol-based formulations' photo-crosslinking with various co-monomers or co-crosslinkers.

Despite the widespread use of panthenol as a bioactive molecule in the cosmetic industry, to the best of our knowledge, panthenol-based macromolecules have not yet been reported. D,L-Panthenol has a melting point of 63.3 °C and a boiling point of 120 °C at 0.02 mmHg [29]. Nevertheless, its low degradation temperature (Sup. Info., Fig. S6) limits polymerization strategies involving conventional organometallic catalysts - step-growth polymerization catalyzed by tin(II) 2-ethyl hexanoate and other Lewis acid catalysts are typically more effective at higher temperatures [30]. Even if the polymerization was not completely precluded, partial degradation of the monomer compromises the reaction stoichiometry, which is essential for monomers in AA-BB polycondensations. Attempts to polymerize the molecule using the aforementioned Sn catalyst resulted in brownish products, indicating side reactions, such as degradation or oxidation. Consequently, the use of enzymes was considered a promising alternative. Among the advantages of using enzymes are their ability to operate under milder conditions, their selectivity and the lack of toxic residual metals [30].

Herein, the synthesis of PPA was performed through a polycondensation approach using Novozym 435, the immobilized version of CAL-B - the most extensively used enzyme due to its versatility, high catalytic activity, and high thermal stability [17] - as catalyst for the transesterification of panthenol with diethyl adipate. Previous reports [21,22] have shown azeotropic distillation as a highly effective technique in removing volatile by-products in case of AA-BB polycondensations catalyzed by Novozym 435. In these studies, isosorbide – a diol with two chemically distinct secondary hydroxyl groups – was reacted with diesters to produce polyesters, yielding polymers with 40 kDa and copolymers with 15 kDa for 168 h reaction time. For the polycondensation of panthenol, the same synthetic approach was used.

After 16 h of azeotropic distillation, the enzyme was filtered off, the product was precipitated and dried under vacuum. The chemical structure of PPA was investigated and confirmed by ^{1}H NMR (Fig. 2A) – endossed by the NMR spectra of its monomers (Figs. S1 and S2, Sup. Info.) – and Raman Spectroscopy (Fig. 2B). The molecular weight of PPA was evaluated by SEC, revealing the production of oligomers with weight-average molecular weight ($\overline{M_w}$) of 2.2 kDa and number-average molecular weight ($\overline{M_n}$) of 1.5 kDa. This is the first example of panthenyl oligoesters synthesis, opening a wide range of possibilities for creating panthenol-based polymers. Given the low cytotoxicity of panthenol [6,9] and diethyl adipate, the resulting polymers are anticipated to be highly biocompatible.

The absence of branching signals (which were likely to appear around ∂4.8–6.0 ppm from methine hydrogens close to the 2-hydroxyl group) suggests the production of a linear oligomer. The finding was also supported by Diego and co-authors [13]: the group reported a kinetic reaction control using Novozym 435 by reacting D-panthenol with isopropyl acetate in acetonitrile. The transesterification of the secondary hydroxyl group from D-panthenol yielding panthenyl triacetate occurred only after 48 h with a stoichiometric ratio of 9:1 (isopropyl acetate:panthenol), endorsing the excellent enzyme regioselectivity for transesterification. In panthenol, the 2-hydroxyl group is not only secondary but also sterically hindered by two methyl groups and one hydroxymethyl on the adjacent carbon, which impairs its reactivity. Additionally, it is classified as an α-hydroxyamide, and the literature lacks examples of lipase-catalyzed polycondensation involving this type of hydroxyl group.

To incorporate photo-reactive sites, PPA was modified with acrylic moieties. This modification aimed to produce a polymer that, in the presence of a photo-initiator, would provide photo-curable formulations. Thus, PPA was reacted with acryloyl chloride in the presence of triethylamine under N_2 atmosphere. After 16 h of reaction time and work-up steps, acrylated PPA (PPA-AC) was finally produced, purified, and dried under vacuum for 72 h.

This reaction introduces acryloyl moieties on the remaining hydroxyl groups of the PPA structure. It is assumed that, initially, the 4- and 3′-hydroxyl terminal groups of the panthenyl units, being the most reactive, undergo acrylation. This reaction is followed by the acrylation of secondary 2-hydroxyl groups from panthenyl, which were less prone to attack the carbonyl group. By adjusting the amount of acryloyl chloride added, it is possible to control the degree of acryloyl substitution, allowing for the tuning of the final product's properties.

Acrylation was attested by the partial downfield shift of the hydrogen signal of the carbon labeled as "g" from panthenol and, unequivocally, by the presence of the set of olefinic hydrogen signals in the ^{1}H NMR spectrum in Fig. 2A (and Fig. S3, Sup. Info.). The presence of unsaturations was further confirmed using MALDI-TOF (Figs. S4–S5, Sup. Info) and Raman Scattering Spectroscopy: Fig. 2B shows clearly the presence of double bonds in the modified PPA. It is possible to observe the appearance of the band corresponding to unsaturation (ν(C=C)) for PPA-AC at 1640 cm^{-1} (yellow shadow). It is important to note that the wider band at 1650 cm^{-1} corresponds to the ν(C=O) stretching from amide in panthenol, which is present either in PPA and PPA-AC. The band at 1725 cm^{-1} is attributed to carbonyl groups from esters, present in both polymers. Additionally, a small shoulder at 3100 cm^{-1} in the red curve can be assigned to the (=C-H) stretch vibration.

It is assumed that in the structure of PPA, each panthenol monomer contains one unreacted secondary hydroxyl group. This assumption relies on the great difference in reactivities from primary 4- and 3′-hydroxyl and secondary 2-hydroxyl groups [13], preventing acrylation and branching. In macromolecules in which panthenol is the end-monomer, a primary hydroxyl terminal would also be present. Due to the differences in reactivity between these types of hydroxyl groups as

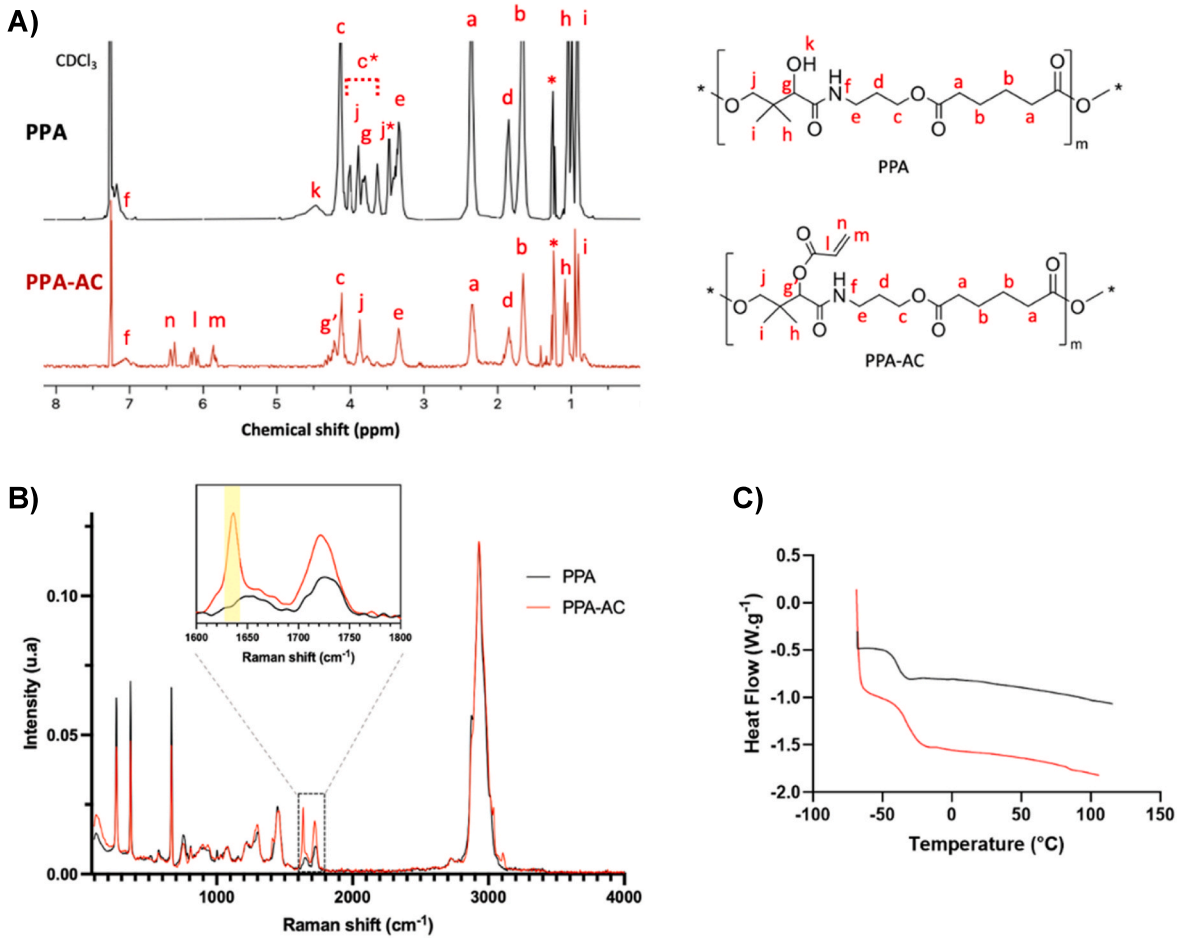

Fig. 2. A) ^{1}H NMR spectra of PPA and PPA-AC; **B)** FT-Raman spectrum of PPA and PPA-AC; **C)** DSC curves for PPA and PPA-AC.

nucleophiles in nucleophilic addition reactions to carbonyl groups, it is anticipated that the terminal primary hydroxyl groups would readily undergo acrylation, followed subsequently by the secondary ones. Using ^{1}H NMR spectroscopy, the PPA-AC structure was verified by identifying characteristic signals in the olefin region, with the degree of unsaturation estimated at approximately 67 % (Sup. Info). Achieving 100 % of substitution was not intended due to the following reasons: (1) it could potentially increase brittleness in the final networks; (2) the amount of unreacted hydroxyl groups helps the control of the hydrophilic character of the final network, or (3) these groups can be further functionalized for additional applications (such as attaching of peptides, growth factors or bioactive drugs).

Thermogravimetric analysis results showed that PPA-AC polymers resist to thermal degradation until 160 °C (Fig. S7, Sup. Info). DSC analysis with a second heating cycle was chosen to evaluate the thermal behavior of the polymer. The curves revealed that PPA and PPA-AC are completely amorphous polymers with a glass transition temperature (T_g) value around −38 °C and −32 °C, respectively (Fig. 2C). The lack of crystallinity is especially relevant as it relates to faster degradations kinetics (vide infra) [31].

3.2. Photo-crosslinking of PPA-AC-based systems

As aforementioned, photo-curable formulations are typically constituted by a mixture of oligomers, photo-initiator, solvent, and other additives, such as co-crosslinkers and photo-absorbers (in case of SLA and DLP). The materials' chemical nature is primarily responsible for its properties (e.g., swelling, resorption kinetics, comprehensive and tensile strength, cell adhesion, etc) [4]. Tuning the proportions of each resin component is a challenging task. Beyond the polymer's physico-chemical characteristics, the choice of the solvent, photo-initiator, and co-crosslinkers are crucial for the successful formation of photo-crosslinked networks.

Photo-crosslinking of acrylates is based on chain-growth polymerization. The initial step of this reaction is the initiation, a process that can be triggered by heat or light if a suitable initiator is added. Typically, non-aromatic molecules are not readily sensitive to light, and a photo-initiator is necessary to trigger free radical chain reactions. In the context of this study, acrylic moieties on the polymer subsequently undergo free-radical polymerization to form a covalently crosslinked network. The rate of photo-polymerization is strongly determined by the photo-initiator, solvent, and light intensity [4]. Numerous studies have described the photo-initiator dependence of photo-curable systems, often using complex equations [4,32]. Bagheri and co-workers [33] have shown different photo-initiators used in photo-polymerization systems.

Herein, three key factors were decisive in selecting a photo-initiator: (i) low cytotoxicity to serve biomedical applications – according to the literature; (ii) the ability to absorb a significant amount of the emitted light from the source; (iii) solubility in the same solvent as the polymer and co-monomers/co-crosslinkers. In view of these requirements, BAPO (bis(2,4,6-trimethylbenzoyl)-phenylphosphineoxide) and TPO-L (ethyl (2,4,6-trimethylbenzoyl) phenyl phosphinate) were considered. The selections of the photo-initiator and solvent were made simultaneously, considering the overall reactivity of the systems.

Given that PPA-AC is a novel polymer, its solubility in different solvents had to be assessed. The polymer was found to be soluble in chlorinated solvents, amides, sulfoxides, and alcohols, and insoluble in hydrocarbons, water, and esters. Despite the suitability of chloroform

and THF to dissolve the material, their high vapor pressures could lead to solvent evaporation in some potential applications such as 3D printing. To avoid this risk, solvents with relatively lower vapor pressures were considered for the tests (Sup. Info., Table S4), including 1,2-dichloroethane (DCE), dimethyl sulfoxide (DMSO), 2-butanol (2-BuOH), and N-methyl-2-pyrrolidone (NMP). PPA-AC was evaluated in terms of its gelation point (by means of photo-rheology). Both BAPO and TPO-L were tested in DCE, DMSO, NMP, and 2-BuOH. The combination of BAPO and DCE was chosen, since it was proven to be the most successful, with the fastest gelation (Sup. Info., Fig. S9).

The curing process is highly influenced by the relative rate of radical formation. In a photo-crosslinking reaction, as the reaction progresses, there is a noticeable increase in the molecular weight and polydispersity of branched molecules. This results in a decrease in the mobility of reactive groups within the polymer chains, making them less available for further reactions [34]. To address the challenge of macroradical diffusion within the medium, different strategies may be employed: (i) it is possible to use solvents to reduce the overall medium viscosity or (ii) typically a small unsaturated compound can be introduced for mobility: a co-monomer (with one double bond) or a co-crosslinker (with two or more double bonds). The addition of a co-monomer or a co-crosslinker improves the overall reactivity of the system. This improvement is particularly significant for less reactive double bonds, such as those found in ethylene 1,2-disubstituted compounds. In this work, these reactive additives were not only employed to enhance reactivity (acrylates are sufficiently reactive) but to impart specific properties to the network in terms of hydrophilicity, surface energy, degradability and mechanical behavior.

In this work, the use of distinct co-monomers and co-crosslinkers (NIP, NVP, VIM, HEX, DVA) was driven by the goal of broadening the formulation landscape and, consequently, expanding the structural and functional diversity of the resulting networks. These additives were chosen for their high reactivity in free-radical polymerization and their demonstrated biocompatibility in analogous systems [35–40]. Their selection was also guided by the objective of assessing how the hydrophilic nature of NIP, NVP, and VIM, in contrast to the hydrophobic characteristics of DVA and HEX, would shape key materials outcomes, such as the hydrolytic degradation and cellular responses. In addition, vinylic monomers containing one or two vinyl groups may undergo different reaction pathways, affecting the final mechanical properties as well as crosslinking efficiency, kinetics, and density. By modifying the formulations with each additive, tunable network properties could be achieved. In addition, NIP and NVP, in particular, had been successfully employed in our group's previous investigations [41].

It is important to note that most unreacted free monomers may present some toxicity due to their reactive double bonds. After the curing process, however, complete conversion is targeted (and reached, vide infra), significantly reducing any potential cytotoxicity of these additives [42].

Three distinct networks (Fig. 3) were produced via light-initiated chain growth polymerization of the acrylate moieties: (A) in the absence of reactive additives, yielding a homopolymer of PPA-AC; (B) through copolymerization of PPA-AC with co-monomers containing a single vinylic functionality (NIP, NVP, and VIM); and (C) through copolymerization of PPA-AC with co-crosslinkers bearing two acrylic functionalities (DVA and HEX). In order to investigate the photo-crosslinking efficiency for these different systems, the covalently crosslinked networks produced were assessed by means of photo-rheology, gel fraction studies, Raman spectroscopy, and HR-MAS ^{1}H NMR spectroscopy.

It is well established that photo-initiated reactions involved in the network formation play a crucial role in determining materials' mechanical characteristics. During a photo-crosslinking reaction, it is possible to observe differences in the materials' viscoelastic behavior before and after light exposure. Photo-rheology can be a powerful tool to investigate the kinetics of curing and the final crosslinked network density. The storage (G′) and the loss moduli (G″) represent, respectively, the elastic response (energy storage), and the viscous response (energy dissipation). Precursor PPA-AC formulations were prepared with different co-monomers and co-crosslinkers. From Fig. 4A, it was possible to analyze the photo-crosslinking kinetics results for these different systems.

Typically, during a photo-rheology evaluation, before light exposure, the rheological properties remain almost constant, reflecting the uncrosslinked state of the mixture. From 60 s onwards, the light exposure begins, so the photo-initiator can absorb light, generating free radicals that start the crosslinking reaction. The rate of photo-polymerization depends on radical diffusion and concentration in the

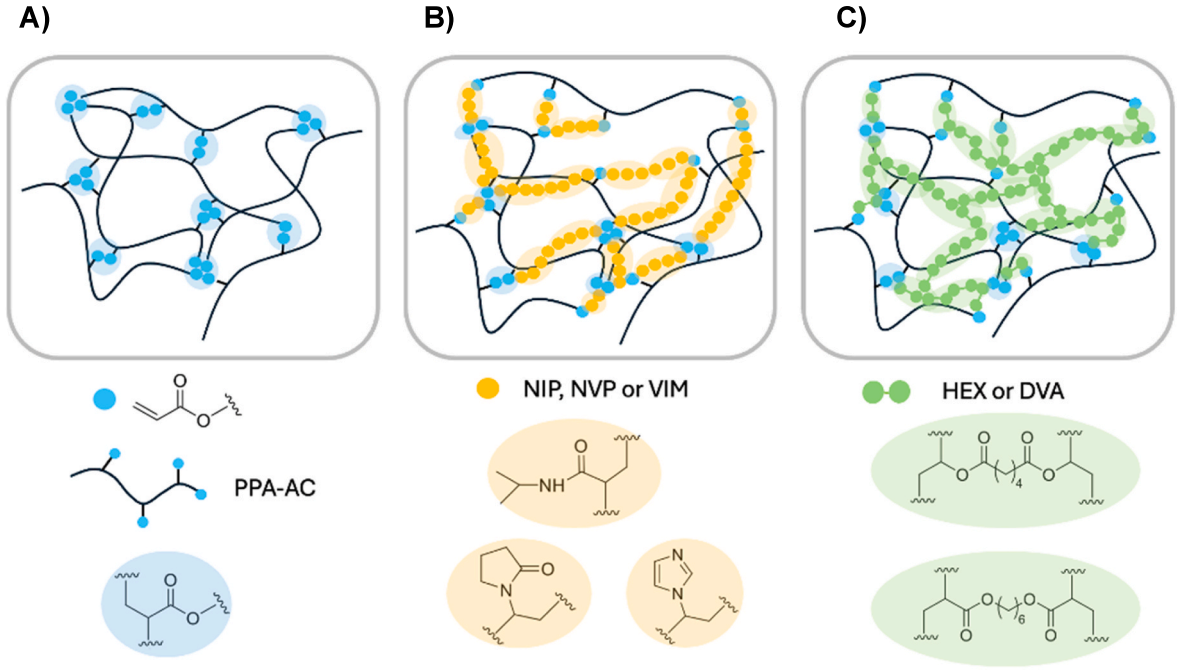

Fig. 3. Schematic representation of networks after photo-crosslinking: **A)** For PPA-AC; B) For PPA-AC + co-monomer; and C) For PPA-AC + co-crosslinker.

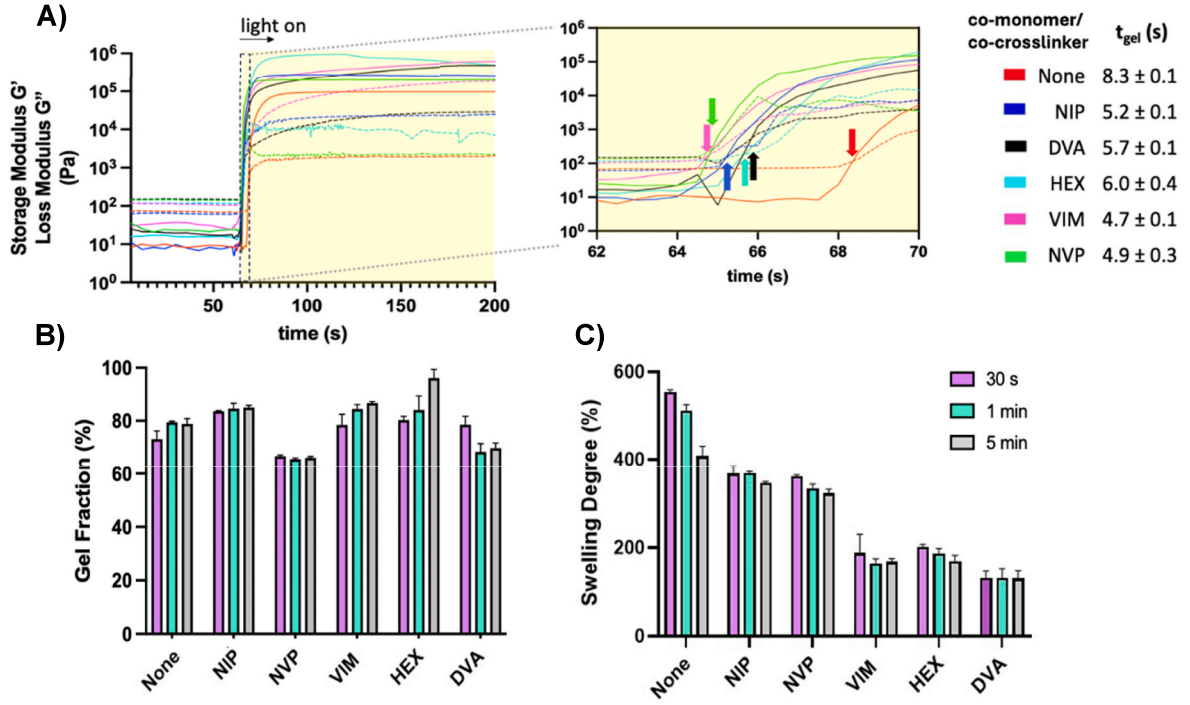

Fig. 4. A) Kinetics of photo-crosslinking analyzed by photo-rheology (irradiation starting after 60 s, wavelength 400–500 nm, 27 mW cm^{-2}). Solid and dashed lines represent, respectively, storage (G′) and loss moduli (G″). A zoom illustrates on the right the gel points (t_{gel}, indicated by arrows); **B)** Gel Fraction (left) and **C)** Swelling Degree (right) in chloroform of PPA-AC crosslinked networks made with BAPO and different co-monomers or co-crosslinkers, using different times of exposure to light.

medium, as well as the propagation rate (determined by the radical reactivity) [43]. This results in a significant rise in the storage modulus, showing the transition from the viscous to the elastic state. For the system to transition from a liquid-like to a solid-like state (gel), a minimum number of crosslinks must form, which occurs at the gel point, the critical moment at which the crossover between G′ and G″ occurs. As the reaction proceeds and the G′ increases, the material becomes predominantly elastic and usually less able to dissipate energy as heat. After a certain time, the storage modulus reaches a plateau, suggesting that most of the crosslinking is complete and the reaction is nearing completion. At the plateau, the G′ reflects the crosslinked material's maximum mechanical strength and stiffness.

The gelation times for all studied formulations ranged from 4 to 8 s, indicating fast kinetics. The formulation without a co-monomer or co-crosslinker showed the highest gelation time (around 8 s), as its precursor solution had fewer reactive double bonds, resulting in fewer crosslinks and lower network density. All the other formulations had the same concentration of vinylic groups, then the curing kinetics could be directly compared; still, the results are quite similar for all co-monomers or co-crosslinkers, with a difference in terms of gel point of less than 1.5 s in all systems. These formulations are essentially good candidates to be exploited in different light-based 3D printing techniques.

The unsaturated monomers used have different “ene” functionalities (N-vinyl, di-vinyl, di-acrylate, and acrylamides), allowing the production of networks with distinct properties due to their varied reactivities and hydrophilicities. The storage moduli at the plateau, ranging from 10^5 to 10^6 Pa, indicate crosslinked networks with different crosslinking densities. According to the rubber elasticity theory [44], the disparity in terms of G′ should be predominantly attributed to variations in terms of M_c (the number average molar mass between two crosslinks). However, this comparison must be made with caution in this case, as the acrylate networks are inherently non-homogeneous [45] and the gel fractions differ significantly across the systems (vide infra).

PPA is a polyester with end-groups that can be either an ethyl carboxylate or a hydroxyl moiety. Since each panthenol residue has an available secondary hydroxyl group, the resulting PPA-AC should present primary and secondary -OH groups modified via acrylation. Consequently, double bonds can be found either in the polymer backbone or the end groups. Given that the DS is not 100 %, the distribution of these double bonds in the polymer chains cannot be determined. Therefore, defects in the network topology should be expected, i.e., the network is not perfectly uniform.

To better understand the formation of crosslinks, the films obtained were assessed (Fig. 4B and C) in terms of gel fraction (GF) and swelling degree (SD). Gel fraction and swelling assays can help to evaluate the extent of photo-crosslinking reactions since they reflect the degree of crosslinking and interconnectivity between different chains. When formed, films consist of two phases: the sol fraction, composed of macromers not included in the organo-gel network (the soluble part), and the gel fraction, resulting from crosslinks connecting polymer chains, forming an insoluble network at the gel point [34].

Fig. 4B shows that within the same set of samples, longer exposure times led to more crosslinks formed, greater polymer chain interconnectivity, and consequently, a higher GF. Hence, one can expect higher gel fraction values for films exposed for 5 min than for 1 min or 30 s. In general, GF values were greater than 65 % for all cases, with most exceeding 80 %, and some reaching 100 %.

The NVP system showed the lowest GF value, around 65–70 %, yet in photo-rheology it showed G’ in the order of 10^5 Pa, suggesting a densely crosslinked material. This result points to a more heterogeneous network, indicating that a portion of the polymer remains uncrosslinked while some regions or domains are well-crosslinked and contribute to the rigidity (probably regions with different crosslinking densities were formed) [45]. VIM, NIP, and HEX demonstrated to be the most efficient systems, with GF higher than 80 % even with only 30 s of light exposure, indicating nearly complete gelation and successful crosslinking. Conversely, for DVA, extended light exposure resulted in a decreased gel fraction, possibly due to some photo-induced degradation.

The swelling degree (SD) is an essential parameter characterizing gels, especially in biomedical applications. In this study, the films

consisted of organogels, and the SD was first measured in chloroform to gain deeper insight into the crosslinked networks produced. Swelling behavior reveals the mechanistic dynamic comprehension of the solvent diffusion process into the gels, indirectly measuring crosslinking density. Swelling can also vary with other factors, such as ionic strength, temperature, and solvent composition [46]. When the solvent is absorbed, the network swells, assuming an elongated configuration between crosslinks. The swelling theory explained by Flory-Rehner affirms that the state of equilibrium swelling is reached when the osmotic forces (driving solvent into the network) are counteracted by the elastic retractive forces (the network chains trying to resist expansion) [47].

The SD tends to decrease as the GF increases due to the more significant number of crosslinks formed. It makes sense to compare different exposure times (30 s, 1 min, or 5 min) within the same set of samples (which consist of the same system). However, this relationship is not necessarily consistent among the co-monomers or co-crosslinkers since the swelling depends not only on the number of crosslinks but also on the distance between them (M_c) and on the solvent-polymer interaction parameter (χ) [48].

Notably, regarding SD values (Fig. 4C), the sample without additives is expected to present higher degrees of swelling, as the absence of co-monomers or co-crosslinkers provides, comparatively, the formation of fewer and possibly more distant crosslinks, i.e., higher M_c (Fig. 3). The systems with HEX, DVA, and VIM showed the lowest SD values, Interestingly, even considering that the chemical nature of each additive is different, these results are consistent with the photo-rheology results (Fig. 4A), where these samples also showed the highest plateau storage modulus and, therefore, higher crosslinking density.

Raman spectroscopy and HR-MAS ^{1}H NMR spectroscopy were performed to evaluate the double bond consumption. In Fig. 5A, PPA-AC (orange curve) exhibits a prominent band around 1645 cm^{-1}, attributed to the symmetric stretching of C=C bonds within the acrylic group of PPA-AC. The process of crosslinking initiated upon light exposure results in the total consumption of these double bonds in all cases, as indicated by the absence of corresponding bands, even in the sample without co-monomers or co-crosslinkers (see enlarged region). Raman analysis unequivocally confirms the successful light-induced crosslinking reactions. These films were also analyzed by ^{1}H NMR spectroscopy (Fig. 5B) in the solvent-swollen state under magic angle spinning parameters (HR-MAS). This quantitative technique revealed the absence of any detectable signals related to acrylate double bonds between 6 and 6.5 ppm (yellow region), indicating a highly efficient free-radical polymerization with full conversion of double bonds in all cases.

3.3. Mechanical properties of PPA-AC crosslinked networks

Constructs' mechanical properties are crucial for scaffold functionality in tissue engineering. A tissue substitute must match the biomechanical characteristics of the tissue it replaces. This compatibility ensures structural integrity and supports proper cellular interactions and tissue regeneration [49].

The stiffness of a material is quantified by the Young's modulus (or the modulus of elasticity), a mechanical property defined as the ratio of stress (force per unit area) to strain (relative deformation) within the material's elastic region. A higher Young's modulus indicates a stiffer material that undergoes minimal deformation under stress. According to Guimarães and co-authors [49] elastic moduli of biological tissues vary widely, ranging from as low as 11 Pa (intestinal mucus) to as high as 20 GPa (cortical bone), depending on the tissue type. Softer tissues such as the cornea, kidney, brain, and cardiac muscle exhibit Young's moduli within the kPa range. Intermediate structures like cartilage have moduli in the MPa range, while denser tissues like bone reach up to the GPa range, reflecting their substantial stiffness and resistance to deformation [49].

To evaluate the mechanical behavior of crosslinked films, Dynamic Mechanical Analysis (DMA) was performed. The Young's Modulus, elongation at break and fracture strength were the properties assessed for each material (Fig. 6).

The results in Fig. 6A and B showed that the values of Young's Moduli, for all samples, are in the range of 4–44 MPa, which highlights the tunability of the materials. This modulus increases with the stiffness of the crosslinked film, resulting in less material deformation. The films obtained with NIP, HEX, and VIM are the stiffest, with average values of 43, 29, and 22 MPa, respectively. Interestingly, the film with DVA is less rigid than the PPA-AC network itself. While it is possible to compare the rigidity of the samples, comparing them solely based on crosslinking density might be misleading: even though the Young's Modulus and the crosslinking density may be directly related (in the rubbery state), this condition holds true primarily for ideally perfect homogeneous networks. Herein, it is hypothesized that the final stiffness of the materials is influenced not only by the M_c but also by factors such as the homogeneity of the newly formed crosslinks, the structure of the co-monomers and co-crosslinkers used, and the gel fraction of each system.

Some articles highlight crystallinity as a crucial factor regarding Young's Modulus [50,51]. Although PPA-AC is entirely amorphous, it cannot be assumed that its photo-crosslinked networks, incorporating of a diversity of reactive additives, retain this amorphous nature. To assess whether crosslinking induced the formation of crystalline regions in the

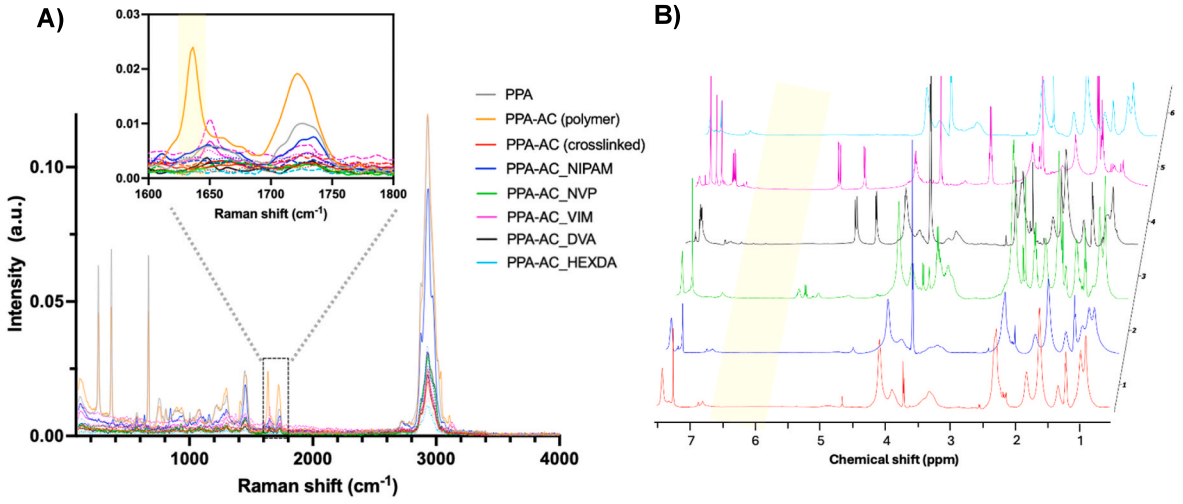

Fig. 5. **A)** Raman spectra of PPA-AC crosslinked networks after 30 s, 1 min or 5 min of light exposure; a zoom illustrates the region of interest. **B)** HR-MAS ^{1}H NMR spectra of the crosslinked films; the yellow shadow shows no signals corresponding to residual double bonds from acrylates.

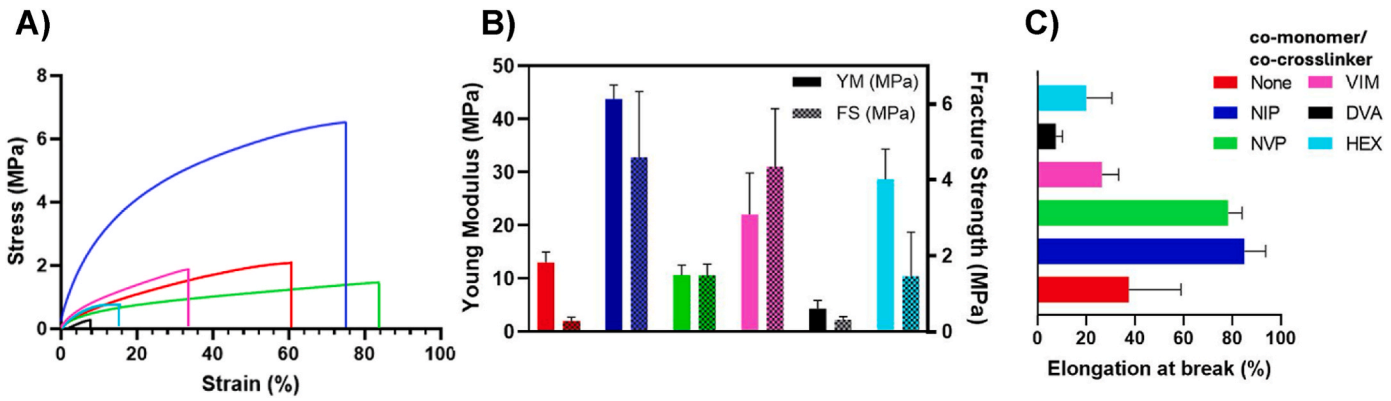

Fig. 6. A) Stress vs. Strain curves for various PPA-AC networks; **B)** Young's Modulus (YM) and Fracture Strength (FS) of crosslinked films; **C)** Elongation at break for networks formed with different co-monomers/co-crosslinkers.

networks, the films were also analyzed by DSC (Fig. S8, Sup. Info.). Similarly to the original polymer, all networks were found to be completely amorphous, with the glass transition being the only thermal event detected during the analyses. Consequently, the diversity of Young's Moduli presented is not a consequence of crystallinity. Nevertheless, one can note a correlation between the elastic modulus and the gel fraction of the films: networks with higher gel fractions (with HEX, NIP, and VIM) also presented a stiffer behavior. This can be attributed to the higher amount of polymer in fact incorporated into the gel's structure, leading to a higher number of crosslinks formed.

Additionally, the chemical nature of the formulation components may also affect the Young's Modulus: co-monomers or co-crosslinkers that are capable of forming hydrogen bonds may exhibit increased stiffness [52,53]. NIP, as an amide, demonstrates strong potential for hydrogen bond formation (both with itself and with the polymer, which is also a polyamide) due to the presence of both a hydrogen bond donor (the -NH group) and a hydrogen bond acceptor (the carbonyl oxygen). It is hypothesized that this property might contribute to the greater rigidity observed in the network containing NIP. The other co-monomers and co-crosslinkers can also participate in hydrogen bonding, but they have only hydrogen bond acceptor groups (the carbonyl oxygen or the imine nitrogen) that would not engage in strong intermolecular hydrogen bonding.

The addition of unsaturated monomers to the PPA-AC formulations represented an advantage in the percentage of elongation at break in networks with NIP and NVP that are at least twice as ductile. In contrast, the incorporation of VIM, HEX, and DVA produced more brittle networks (Fig. 6C). Films with higher crosslinking densities were less ductile, which can be attributed, in this case, to a restricted network mobility and inhomogeneity of the new crosslinks in these systems. Interestingly, the addition of NIP represented a gain in both stiffness and flexibility, which might be related to the ability of hydrogen bonds to rearrange: in some cases they can break during deformation and subsequently reform, increasing the material's extensibility [54].

The rupture stress values for all films are low, with each being less than 5 MPa, indicating that the networks sustain minimal stress. As previously discussed, acrylate photo-crosslinked networks are formed by uncontrolled chain-growth polymerization, which causes spatial inhomogeneity and defects within the network architecture [45]. A more homogeneous network generally distributes stress more effectively, which would probably mean a better reorientation of crosslinks during the stretching process [55].

3.4. Contact angle and surface energy of PPA-AC crosslinked networks

Contact angle measurements provide valuable information about the wettability of a surface, indicating its ability to facilitate or resist the spread of a liquid droplet. This characteristic arises from intricate intermolecular interactions between the liquid's surface tension components and the physical-chemical properties of the surface being tested [56]. This type of evaluation is highly relevant since the hydrophilic/hydrophobic behavior of a novel material is essential for validating its suitability for specific applications. For instance, the first stage of implant recognition involves the innate immune system initiating the adsorption of plasma proteins on the implant's surface. This very complex process varies with the characteristics of the implantation surface, such as hydrophilicity, topography, roughness, chemical structure, and tension [57]. Consequently, knowing the materials' surface energy is crucial for predicting their optimal performance, particularly regarding degradation kinetics, cell adhesion and proliferation [58]. Moreover, this understanding enables mitigation of undesirable host responses, including thrombosis, inflammation, and infections, thereby improving the biocompatibility and overall efficacy of the implanted material [56]. The results presented in Table 1 refer to flat sheet surfaces.

Table 1 reveals that all contact angles measured for water were below 60°. Static water contact angle readings below 65° indicate surfaces with hydrophilic characteristics [59]. This result aligns with expectations, given the chemical composition of the polyester formed by panthenol (a highly hygroscopic molecule containing amide groups) and diethyl adipate. The film made solely by PPA-AC and BAPO has a Θ_{water} of (52.7 ± 1.5)°, being more hydrophilic than other traditional and well-established polyesters explored in biomedical applications, such as poly(ε-caprolactone) [60] and poly(L-lactic acid) [61].

The variations in contact angle measurements for water among different co-monomers or co-crosslinkers are less pronounced. However, the sample containing HEX exhibited the highest Θ_{water}, which was already expected considering HEX's greater hydrophobic nature due to its longer carbon chain. This observation highlights the potential for tuning surface hydrophobicity by manipulating the alkyl chain length of the crosslinker. Conversely, the lowest Θ_{water} value was recorded for NVP, consistent with its highly polar and hydrophilic nature. These findings are corroborated by surface energy measurements, with NVP demonstrating the most significant polar components (both acid γ^{+} and basic γ^{-}), and DVA and HEX exhibiting higher dispersive components and hydrophobic character.

The values obtained with glycerol, a very polar liquid, show trends similar to those of water. Diiodomethane is a liquid with nonpolar character and, therefore, should spread more on hydrophobic surfaces – in contrast with the other analyzed solvents. The results, however, are not in agreement with those when using water and glycerol. Generally, the drops spread more, making the measurement more challenging to analyze, which may have led to such inconsistencies.

Cell adhesion is an extremely complex process affected by the type of cells and environmental factors, such as surface free energy, electrostatic interaction, steric repulsion, hydration, and topography [62]. As explained by Lih, cell adhesion tends to be lower on substrates with a

Table 1
Contact angle measurements and surface energy calculations for crosslinked films.

co-monomer/co-crosslinker	Θ_{H_2O} (deg)	$\Theta_{glycerol}$ (deg)	$\Theta_{CH_2I_2}$ (deg)	Υ^{LW} (mJ m^{-2})	Υ^{-}(mJ m^{-2})	Υ^{+} (mJ m^{-2})	Υ_S (mJ m^{-2})
none	52.7 ± 1.5	54.7 ± 2.3	21.7 ± 2.5	47.3 ± 0.8	27.1 ± 0.7	0.01 ± 0.01	48.0 ± 1.4
NIP	52.7 ± 2.1	56.3 ± 4.9	30.7 ± 1.2	44.0 ± 0.5	29.9 ± 5.7	0.11 ± 0.08	47.4 ± 1.2
DVA	53.7 ± 4.6	57.0 ± 1.7	20.3 ± 2.1	47.7 ± 0.6	8.5 ± 2.6	5.17 ± 0.07	60.7 ± 1.8
VIM	55.3 ± 1.2	57.0 ± 2.0	23.0 ± 1.0	46.8 ± 0.3	22.7 ± 2.2	0.02 ± 0.02	47.9 ± 1.1
HEX	58.7 ± 2.7	59.7 ± 1.5	23.7 ± 1.2	46.6 ± 0.4	24.1 ± 4.7	0.06 ± 0.01	48.6 ± 2.5
NVP	49.0 ± 8.2	54.3 ± 2.1	25.7 ± 4.7	45.8 ± 1.8	32.5 ± 10.3	0.02 ± 0.02	47.3 ± 2.5

low surface free energy substrate compared to those with high surface free energy. For significant cell adhesion to occur, Υ_S values must be higher than 43 mJ cm^{-2}, which applies to all systems studied here [62].

3.5. Hydrolytic degradation of PPA-AC crosslinked networks

The potential of biomaterial biodegradability is pivotal in the context of regenerative medicine, as it is targeted that the biodegradation rate is in line with the rate at which new tissue is formed. In this regard, the intrinsic features of materials and the host response are crucial in determining the successful clinical outcome. While there is no established benchmark for panthenol-based polymers, it is widely known that polyesters undergo hydrolytic degradation through the random scission of ester bonds. Several network-related properties influence the degradation profile, including hydrophilicity, crosslinking density, and crystallinity [31,57].

Typically, water penetration is more pronounced in less crystalline polymer networks, as the amorphous regions allow for more efficient water diffusion. This principle applies similarly to hydrophilic materials, in which the affinity for water further enhances penetration into the matrix [57,63].

Given that PPA-AC is a hydrophilic and amorphous oligoester, fast degradation kinetics could be anticipated. The photo-crosslinked films' degradation rate profiles (Fig. 7) were evaluated under accelerated conditions (0.05 M NaOH, 37 °C) and in PBS at 37 °C (simulating the physiological conditions).

Fig. 7A shows that, under accelerated conditions, the networks undergo near-complete degradation within 7 days – reaching up to >95 % of mass loss for films with no or with hydrophilic co-monomers (NIP and NVP, which showed very similar degradation profile). The degradation kinetics were much slower for networks produced with more hydrophobic co-crosslinkers, such as DVA and HEX, which also had similar profiles. It is worth noting that the system without co-monomers/co-crosslinkers was the first one to be fully degraded since it had fewer covalent crosslinks. Under basic conditions, the degradation is primarily chemically driven rather than diffusion limited. However, the water uptake capacity is still relevant. The incorporation of co-monomers/co-crosslinkers adds new functional groups to the network (amides, imines, or more ester groups) that will degrade differently. Imines are much less stable than carbonyl derivatives and are usually more prone to hydrolysis which might also explain the initial faster degradation of the system with VIM.

Although the hydrolytic degradation of polyesters can take several months under physiological conditions, the materials' degradation rate in PBS at 37 °C (more closely resembling physiological conditions) may be crucial in guiding the selection of suitable final applications for the biomaterials. Under this condition, mass loss ranged from approximately 18 %–30 % over 2 months (Fig. 7B). Once again, the networks containing NIP and NVP exhibited nearly indistinguishable degradation profiles, as did those with DVA and HEX.

Under neutral conditions, the degradation is much slower and more guided by water diffusion. Considering that water sorption into the network is essential for bulk hydrolysis, the degree of swelling in water (Fig. 7C) was also assessed for each network. The systems that swelled more (with NIP, NVP, and VIM) presented faster degradation. In this case, the lower number of crosslinks in the network with no co-monomer or co-crosslinker may be compensated by the hydrophobic character of the network.

Given that all the networks produced were found to be entirely amorphous, the findings suggest that the water uptake capacity and hydrophilicity of the final networks (strictly related to the nature of the co-monomer or co-crosslinker) governs the degradation rate, playing a more substantial role than the crosslink density (that followed another trend). In general, more hydrophobic co-crosslinkers resulted in polymer networks with lower affinity for water, which allows fewer water molecules to penetrate into the networks, decreasing the likelihood of hydrolysis.

To summarize, these outcomes show that it is possible to design panthenol-based materials with tailored degradation rates for specific applications by changing the hydrophilic nature of the co-monomer/co-crosslinker and overall network, in agreement with the aspects discussed in previous sections. While we do not yet have a complete degradation profile for these materials under real physiological conditions, it is plausible to anticipate that panthenol-based oligoesters (hydrophilic

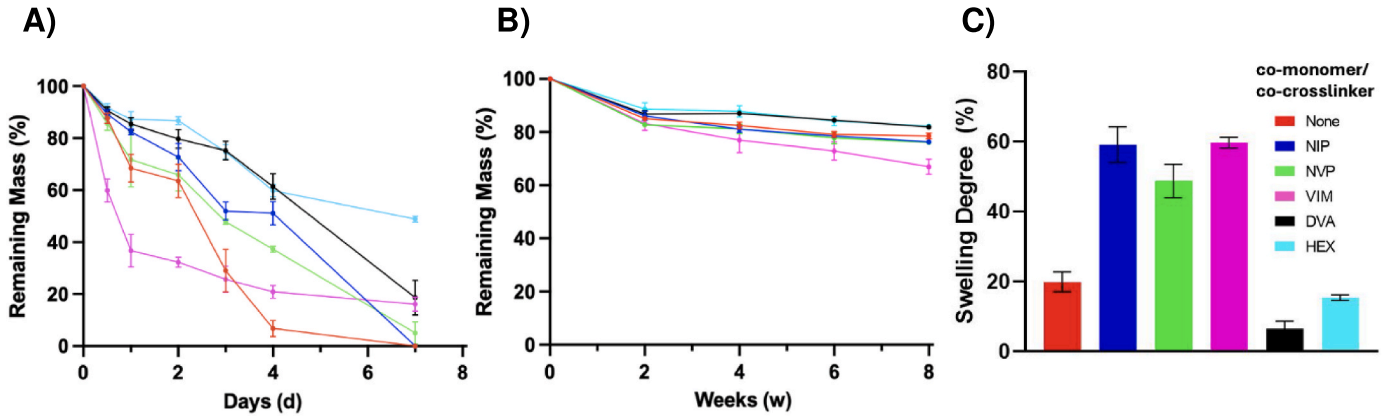

Fig. 7. Hydrolytic degradation in **A)** NaOH 0.01M, and **B)** under physiological conditions (PBS, 37 °C) of photo-crosslinked PPA-AC discs. **C)** Swelling degree (%) in water of the photo-crosslinked PPA-AC discs.

and amorphous) would degrade more rapidly compared to other well-known synthetic polyesters, such as poly(ε-caprolactone) [64], poly (lactides) [64], and poly(globalide) [65] that are known for their longer degradation terms.

3.6. Direct cytotoxicity of PPA-AC crosslinked networks

Direct cytotoxicity tests were performed on the films to evaluate the biocompatibility of the developed polymers. For this, the trypan blue exclusion assay – a classic method for differentiating live from dead cells based on the integrity of the plasma membrane – was performed. First, the cell line NIH-3T3 (mouse embryonic fibroblasts) was placed in contact with each crosslinked film for 3 or 7 days. After staining with trypan blue, the viable and non-viable cells were count with a Neubauer chamber (Fig. 8). It is worth to say that fibroblasts, such as NIH-3T3, are the most important cell type in connective tissue, producing extracellular matrix components and different types of collagens [66].

After 3 days of contact, higher cell viability was observed for the films of the crosslinked polymer without vinylic monomer (∅) and for those containing VIM and NIP. After 7 days, a high number of viable cells was still observed for NVP, VIM, and HEX, indicating not only cell survival but also proliferation. In the case of the VIM-based material, the results demonstrate its superior capacity for cell adhesion, establishing it over time as a promising biocompatible material. The findings reveal its ability to serve as a surface that supported cell proliferation to more than 100 % of the cell number observed in the control.

The results obtained indicate that, as expected, the choice of vinylic additive in the network can elicit significantly different cellular responses. Overall, it can be concluded that biocompatible materials can be produced from the panthenol-based polymer crosslinked with NVP, VIM, and HEX, with the VIM network exhibiting the most favorable cellular behavior. It is important to note that the films analyzed were not subjected to any prior surface modification treatment to enhance cell adhesion, which could be explored in future studies for those materials that did not demonstrate sufficient biocompatibility.

Given the established biocompatibility of panthenol and the safety of diethyl adipate as a co-monomer, it was anticipated that panthenol-based polymers could form biocompatible networks. Additionally, the selected co-monomers and co-crosslinkers, as previously noted, are components of other biocompatible systems. Therefore, the systems investigated in this study were expected to be non-toxic. Although these assays represent a highly simplified *in vitro* assay compared to the complexity of the *in vivo* environment [57], the results of the studies provide a valuable initial assessment of the safety profile of the panthenol-based materials.

4. Conclusion

For the first time in the literature, unprecedented panthenol-derived oligomers have been successfully synthesized, modified, and photo-crosslinked. Enzyme-catalyzed polycondensation was employed to synthesize PPA of low molecular weight (around 2 kDa). By modifying the hydroxyl groups, the oligoester was acrylated, resulting in an amorphous polymer with around 67 % double bond functionalization. Various co-monomers or co-crosslinkers were added to PPA-AC to create photo-curable formulations, allowing for fine-tuning of the photo-crosslinked network properties.

These systems demonstrated exceptional efficiency in photo-curing, achieving high network densities with rapid gelation kinetics (faster than 5 s). The formation of a covalently crosslinked network was unequivocally confirmed by Raman Spectroscopy and HR-MAS ^{1}H NMR spectroscopy, as evidenced by the disappearance of unsaturation signals after the curing process. These formulations are highly effective in photo-crosslinking, making them promising candidates for scaffolds produced via light-based biofabrication techniques. The systems have proven to be hydrolytically degradable, with tailored degradation rates, and show great promise in biocompatibility, being non-toxic for the cell line tested (NIH-3T3). The incorporation of distinct co-monomers and co-crosslinkers endowed the resulting materials with a key feature for tissue engineering applications: a high degree of tunability. This allowed for fine adjustment of chemical, physical, and biological properties in order to match the requirements of different tissues. Moreover, the use of panthenol as a novel monomer for polycondensation, alongside with the potential to further modify panthenol-derived polymers with diverse unsaturated groups or bioactive molecules, opens up exciting possibilities for their use across diverse biomedical applications.

CRediT authorship contribution statement

Isabela Lima Autran Dourado: Writing – review & editing, Writing – original draft, Visualization, Methodology, Investigation, Data curation, Conceptualization. **Daniel Franco Minatelli:** Methodology, Investigation, Conceptualization. **Anna Szabó:** Writing – review & editing, Methodology, Data curation. **Denisse Esther Mallaupoma Camarena:** Data curation, Investigation, Methodology, Validation, Writing – review & editing, Conceptualization. **Flávia Gonçalves:** Methodology, Investigation, Data curation. **Sandra Van Vlierberghe:** Writing – review & editing, Supervision, Resources. **Luiz Henrique Catalani:** Writing – review & editing, Supervision, Resources, Project administration, Methodology, Funding acquisition, Conceptualization.

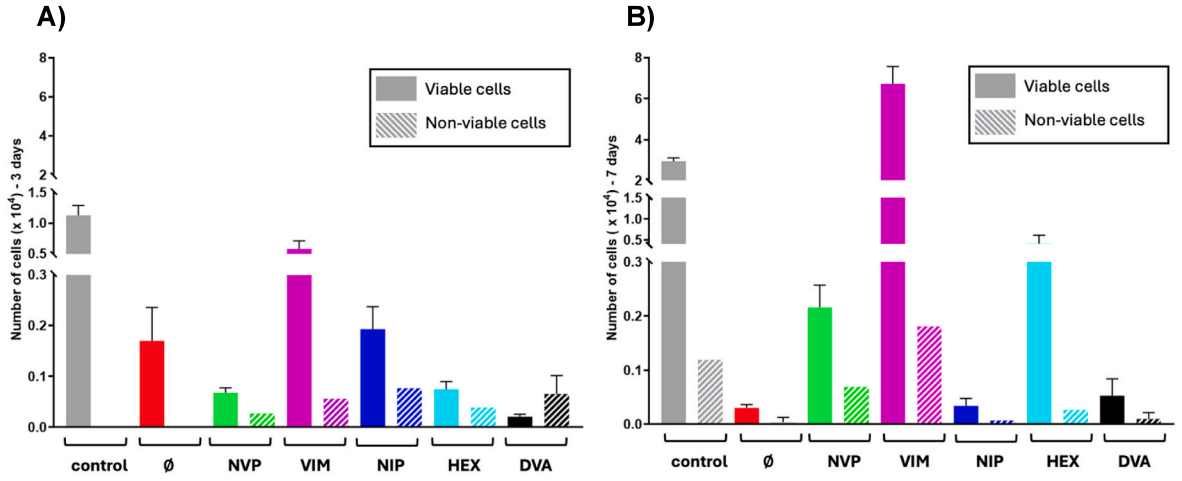

Fig. 8. Cytotoxicity evaluation of NIH-3T3 cells in direct contact with the crosslinked films assessed by Trypan Blue exclusion after **A)** 3 days and **B)** 7 days of incubation. Data show the number of viable (solid shading) and non-viable (hatched shading) cells.

Declaration of competing interest

The authors declare that they have no known competing financial interests or personal relationships that could have appeared to influence the work reported in this paper.

Acknowledgments

The authors are grateful for support received from FAPESP (thematic project #2018/13492-2, FAPESP-FWO project #2024/08578-6, internship abroad #2022/09992-5, and doctorate fellowship #2018/12602-9), CAPES and CNPq for funding this research. The authors are also thankful for the 500 MHz NMR (with the HR-MAS probe) used in this work, which is part of the NMR Expertise Centre at UGent, supported by fundings #01XP2017 (2017) and BOF/COR/2023/006 (2023). Special thanks are extended to Prof. Romulo Ando (IQ-USP) for his assistance with the Raman experiments.

Appendix A. Supplementary data

Supplementary data to this article can be found online at https://doi.org/10.1016/j.mtadv.2026.100686.

Data availability

Data will be made available on request.

References

[1] A. Atala, Tissue engineering and regenerative medicine: concepts for clinical application, Rejuvenation Res. 7 (2004) 15–31, https://doi.org/10.1016/B978-0-12-822944-6.00097-9.
[2] R.J. Mondschein, A. Kanitkar, C.B. Williams, S.S. Verbridge, T.E. Long, Polymer structure-property requirements for stereolithographic 3D printing of soft tissue engineering scaffolds, Biomaterials 140 (2017) 170–188, https://doi.org/10.1016/j.biomaterials.2017.06.005.
[3] A. Kirillova, T.R. Yeazel, D. Asheghali, S.R. Petersen, S. Dort, K. Gall, M.L. Becker, Fabrication of biomedical scaffolds using biodegradable polymers, Chem. Rev. 121 (2021) 11238–11304, https://doi.org/10.1021/acs.chemrev.0c01200.
[4] C. Yu, J. Schimelman, P. Wang, K.L. Miller, X. Ma, S. You, J. Guan, B. Sun, W. Zhu, S. Chen, Photopolymerizable biomaterials and light-based 3D printing strategies for biomedical applications, Chem. Rev. 120 (2020) 10695–10743, https://doi.org/10.1021/acs.chemrev.9b00810.
[5] N. Plesofsky-Vig, Pantothenic acid, in: M.E. Shils, J.A. Olson, M. Shike, A. C.R. (Eds.), Mod. Nutr. Heal. Dis., ninth ed., Lippincott Williams & Wilkins, 1999.
[6] F. Ebner, A. Heller, F. Rippke, I. Tausch, B. Ag, D.C. Clinic, Topical use of dexpanthenol in skin disorders, Am. J. Clin. Dermatol. 3 (2016) 427–433, https://doi.org/10.2165/00128071-200203060-00005.
[7] M.A.M. Shehata, S.M. Tawakkol, L.E. Abdel, Colorimetric and fluorimetric methods for determination of panthenol in cosmetic and pharmaceutical formulation, J. Pharm. Biomed. Anal. 27 (2002) 729–735.
[8] F.B. Camargo, L.R. Gaspar, P.M.B.G.M. Campos, U.D.S. Paulo, Skin moisturizing effects of panthenol-based formulations, J. Cosmet. Sci. 62 (2011) 361–369.
[9] D.L. Bissett, Common cosmeceuticals, Clin. Dermatol. 27 (2009) 435–445, https://doi.org/10.1016/j.clindermatol.2009.05.006.
[10] A. Kabir, M.J. Dunlop, B. Acharya, R. Bissessur, M. Ahmed, Water recycling efficacies of extremely hygroscopic, antifouling hydrogels, RSC Adv. 8 (2018) 38100–38107, https://doi.org/10.1039/C8RA07915C.
[11] F. Lantoine-Adam, R. Letienne, E. Dupont-Passelaigue, Panthenyl Docosahexaeneoate and its Use for Treating and Preventing Cardiovascular Diseases, 2015.
[12] J. Smith, Z. Liu, M. Vedachalam, D. Compton, Process of Making D-panthenyl Triacetate, 2005.
[13] T. De Diego, A. Manjón, J.L. Iborra, Selective synthesis of panthenyl esters by a kinetically controlled enzymatic process, Biocatal. Biotransform. 31 (2013) 175–180, https://doi.org/10.3109/10242422.2013.814644.
[14] S. Nieto, J.M. Bernal, R. Villa, E. Garcia-Verdugo, A. Donaire, P. Lozano, Sustainable setups for the biocatalytic production and Scale-Up of panthenyl monoacyl esters under solvent-free conditions, ACS Sustain. Chem. Eng. 11 (2023) 5737–5747, https://doi.org/10.1021/acssuschemeng.3c00266.
[15] P. Lozano, E. Alvarez, S. Nieto, R. Villa, J.M. Bernal, A. Donaire, Biocatalytic synthesis of panthenyl monoacyl esters in ionic liquids and deep eutectic solvents, Green Chem. 21 (2019) 3353–3361, https://doi.org/10.1039/c9gc01076a.
[16] C. Ortiz, M.L. Ferreira, O. Barbosa, J.C.S. Santos, R.C. Rodrigues, Á. Berenguer-murcia, L.E. Briand, R. Fernandez-lafuente, Novozym 435: the “perfect” lipase immobilized biocatalyst? Catal. Sci. Technol. 9 (2019) 2380–2420, https://doi.org/10.1039/c9cy00415g.
[17] J. Uppenberg, M.T. Hansen, S. Patkar, T.A. Jones, The sequence, crystal structure determination and refinement of two crystal forms of lipase B from Candida Antarctica, Structure 2 (1994) 293–308.
[18] C.H. Kwon, S.W. Kim, Molecular modeling and its experimental verification for the catalytic mechanism of Candida antartica lipase B, J. Microbiol. Biotechnol. 17 (2007) 1098–1105.
[19] C. Ortiz, M.L. Ferreira, O. Barbosa, J.C.S. Santos, R.C. Rodrigues, Á. Berenguer-murcia, L.E. Briand, R. Fernandez-lafuente, Novozyme 435: the “Perfect” Lipase Immobilized Biocatalyst? R. Soc. Chem. 9 (2019) 2380–2420, https://doi.org/10.1039/c9cy00415g.
[20] J. Hu, W. Gao, A. Kulshrestha, R.A. Gross, V. Re, M. Recei, V. August, Sweet polyesters ”: Lipase-Catalyzed condensation - polymerizations of alditols, Macromolecules 39 (2006) 6789–6792.
[21] D. Juais, A.F. Naves, C. Li, R.A. Gross, L.H. Catalani, Isosorbide polyesters from enzymatic catalysis, Macromolecules 43 (2010) 10315–10319, https://doi.org/10.1021/ma1013176.
[22] A.F. Naves, H.T.C. Fernandes, A.P.S. Immich, L.H. Catalani, Enzymatic syntheses of unsaturated polyesters based on isosorbide and isomannide, J. Polym. Sci. Part A Polym. Chem. 51 (2013) 3881–3891, https://doi.org/10.1002/pola.26789.
[23] D.L. Hern, J.A. Hubbell, Incorporation of Adhesion Peptides into Nonadhesive Hydrogels Useful for Tissue Resurfacing, Inc. Adhes. Pept., 1997.
[24] A. Nebioglu, M.D. Soucek, Investigation of the properties of UV-curing acrylate-terminated unsaturated polyester coatings by utilizing an experimental design methodology, J. Coating Technol. Res. 4 (2007) 425–433, https://doi.org/10.1007/s11998-007-9035-y.
[25] A.J. Domb, N. Manor, O. Elmalak, Biodegradable bone cement compositions based on acrylate and epoxide terminated poly(propylene fumarate) oligomers and calcium salt compositions, Biomaterials 17 (1996) 411–417, https://doi.org/10.1016/0142-9612(96)89657-8.
[26] S. Sharifi, M. Imani, H. Mirzadeh, M. Atai, F. Ziaee, Synthesis , characterization , and biocompatibility of novel injectable , biodegradable , and *in situ* crosslinkable polycarbonate-based macromers, J. Biomed. Mater. Res., Part A 90 (2008) 830–843, https://doi.org/10.1002/jbm.a.32138.
[27] C.J. Van Oss, M.K. Chaudhury, R.J. Good, Interfacial Lifshitz-van der Waals and Polar Interactions in Macroscopic Systems, Chem. Rev. 88 (1988) 927–941.
[28] D.Y. Kwok, The usefulness of the Lifshitz-van der Waals/acid-base approach for surface tension components and interfacial tensions, Colloids Surfaces A Physicochem. Eng. Asp. 156 (1999) 191–200, https://doi.org/10.1016/S0927-7757(99)00070-9.
[29] L.N. Scott, M. Fiume, W.F. Bergfeld, D. V Belsito, R.A. Hill, C.D. Klaassen, D. C. Liebler, J.G. Marks, R.C. Shank, T.J. Slaga, P.W. Snyder, B. Heldreth, Safety assessment of panthenol , pantothenic acid , and derivatives as used in cosmetics, Int. J. Toxicol. 41 (2022) 77–128, https://doi.org/10.1177/10915818221124809.
[30] C.D. Fernandes, B.F. Oechsler, C. Sayer, D. Oliveira, P.H.H. De Araújo, Recent advances and challenges on enzymatic synthesis of biobased polyesters via polycondensation, Eur. Polym. J. 169 (2022), https://doi.org/10.1016/j.eurpolymj.2022.111132.
[31] J.C. Middleton, A.J. Tipton, Synthetic biodegradable polymers as orthopedic devices, Biomaterials 21 (2000) 2335–2346.
[32] G. Odian, Principles of Polymerization, fourth ed., Wiley-Interscience, New Jersey, 2004.
[33] A. Bagheri, J. Jin, Photopolymerization in 3D printing, ACS Appl. Polym. Mater. 1 (2019) 593–611, https://doi.org/10.1021/acsapm.8b00165.
[34] K. Dušek, M. Dušková-Smrčková, Network structure formation during crosslinking of organic coating systems, Prog. Polym. Sci. 25 (2000) 1215–1260, https://doi.org/10.1016/S0079-6700(00)00028-9.
[35] C.D. Spicer, Hydrogel scaffolds for tissue engineering: the importance of polymer choice, Polym. Chem. 11 (2020) 184–219, https://doi.org/10.1039/c9py01021a.
[36] I. Matai, G. Kaur, A. Seyedsalehi, A. McClinton, C.T. Laurencin, Progress in 3D bioprinting technology for tissue/organ regenerative engineering, Biomaterials 226 (2020) 119536, https://doi.org/10.1016/j.biomaterials.2019.119536.
[37] A. Mautner, B. Steinbauer, S. Orman, G. Russmüller, K. Macfelda, T. Koch, J. Stampfl, R. Liska, Tough photopolymers based on vinyl esters for biomedical applications, J. Polym. Sci. Part A Polym. Chem. 54 (2016) 1987–1997, https://doi.org/10.1002/pola.28065.
[38] M.G. Chung, H.W. Kim, B.R. Kim, Y.B. Kim, Y.H. Rhee, Biocompatibility and antimicrobial activity of poly(3-hydroxyoctanoate) grafted with vinylimidazole, Int. J. Biol. Macromol. 50 (2012) 310–316, https://doi.org/10.1016/j.ijbiomac.2011.12.007.
[39] D. Espinosa-Hoyos, H. Du, N.X. Fang, K.J. Van Vliet, Poly(HDDA)-Based polymers for microfabrication and mechanobiology, MRS Adv (2017) 6–12.
[40] V. Capella, R.E. Rivero, A.C. Liaudat, L.E. Ibarra, Cytotoxicity and bioadhesive properties of poly- N - isopropylacrylamide hydrogel, Heliyon 5 (2019), https://doi.org/10.1016/j.heliyon.2019.e01474, 1–19.
[41] L.O. Rebouças, I.L.A. Dourado, G. Delechiave, D.E.M. Camarena, S. Van Vlierberghe, L.H. Catalani, Photo-curable resins based on poly(globalide) for 3D printing of resorbable scaffolds: synthesis, crosslinking and post-functionalization, Polymer Chemistry 16 (2025) 2962–2977, https://doi.org/10.1039/d5py00237k.
[42] Y. Murakami, A. Kawata, S. Suzuki, S. Fujisawa, Cytotoxicity and pro-inflammatory properties of aliphatic alpha, beta-unsaturated acid and ester monomers in RAW264.7 cells and their chemical reactivity, *In vivo* (Brooklyn) 33 (2019) 313–323, https://doi.org/10.21873/invivo.11477.
[43] J.P. Fouassier, Photoinitiation, photopolymerization, and photocuring: fundamentals and applications. https://doi.org/10.1109/MEI.1996.546285, 1996.

[44] S.S. Sheiko, A.V. Dobrynin, Architectural code for rubber elasticity: from supersoft to superfirm materials, Macromolecules 52 (2019) 7531–7546, https://doi.org/10.1021/acs.macromol.9b01127.
[45] S. Seiffert, Scattering perspectives on nanostructural inhomogeneity in polymer network gels, Prog. Polym. Sci. 66 (2017) 1–21, https://doi.org/10.1016/j.progpolymsci.2016.12.011.
[46] N.A. Peppas, Physiologically responsive hydrogels, J. Bioact. Compat, Polym. 6 (2015) 241–246.
[47] P.J. Flory, J. Rehner, Statistical mechanics of cross-linked polymer networks II . Swelling, J. Chem. Phys. 521 (1943) 521.
[48] N.A. Peppas, Hydrogels in medicine and pharmacy. https://doi.org/10.1016/0168-3659(89)90068-0, 1989.
[49] C.F. Guimarães, L. Gasperini, A.P. Marques, R.L. Reis, The stiffness of living tissues and its implications for tissue engineering, Nat. Rev. Mater. 5 (2020) 351–370, https://doi.org/10.1038/s41578-019-0169-1.
[50] J. Dong, J. Liu, X. Li, Q. Liang, X. Xu, Relationship between the young's modulus and the crystallinity of cross-linked Poly(ε-caprolactone) as an immobilization membrane for cancer radiotherapy, Glob. Chall. 4 (2020) 1–5, https://doi.org/10.1002/gch2.202000008.
[51] K. Jariyavidyanont, Q. Yu, A. Petzold, T. Thurn-Albrecht, R. Glüge, H. Altenbach, R. Androsch, Young's modulus of the different crystalline phases of poly (L-lactic acid), J. Mech. Behav. Biomed. Mater. 137 (2023), https://doi.org/10.1016/j.jmbbm.2022.105546.
[52] H. Yu, Q. Xiao, G. Qi, F. Chen, B. Tu, S. Zhang, Y. Li, Y. Chen, H. Yu, P. Duan, A hydrogen bonds-crosslinked hydrogels with self-healing and adhesive properties for hemostatic, Front. Bioeng. Biotechnol. 10 (2022) 1–12, https://doi.org/10.3389/fbioe.2022.855013.
[53] C. Xu, Y. Chen, S. Zhao, D. Li, X. Tang, H. Zhang, J. Huang, Z. Guo, W. Liu, Mechanical regulation of polymer gels, Chem. Rev. (2024), https://doi.org/10.1021/acs.chemrev.3c00498.
[54] Z. Zhang, J. Luo, S. Zhao, S. Ge, J.M.Y. Carrillo, J.K. Keum, C. Do, S. Cheng, Y. Wang, A.P. Sokolov, P.F. Cao, Surpassing the stiffness-extensibility trade-off of elastomers via mastering the hydrogen-bonding clusters, Matter 5 (2022) 237–252, https://doi.org/10.1016/j.matt.2021.11.007.
[55] Q. Thijssen, A. Quaak, J. Toombs, E. De Vlieghere, L. Parmentier, H. Taylor, S. Van Vlierberghe, Volumetric printing of thiol-ene photo-cross-linkable Poly(ε-caprolactone): a tunable material platform serving biomedical applications, Adv. Mater. (2023) 2210136, https://doi.org/10.1002/adma.202210136.
[56] G. Agrawal, Y.S. Negi, S. Pradhan, M. Dash, S.K. Samal, Wettability and Contact Angle of Polymeric Biomaterials, Elsevier Ltd., 2017, https://doi.org/10.1016/B978-0-08-100737-2.00003-0.
[57] C. Li, C. Guo, V. Fitzpatrick, A. Ibrahim, M.J. Zwierstra, P. Hanna, A. Lechtig, A. Nazarian, S.J. Lin, D.L. Kaplan, Design of biodegradable, implantable devices towards clinical translation, Nat. Rev. Mater. 5 (2020) 61–81, https://doi.org/10.1038/s41578-019-0150-z.
[58] T.G. Vladkova, Surface engineered polymeric biomaterials with improved biocontact properties, Int. J. Polym. Sci. 2010 (2010), https://doi.org/10.1155/2010/296094.
[59] E.A. Vogler, Structure and reactivity of water at biomaterial surfaces, Adv. Colloid Interface Sci. 74 (1998) 69–117, https://doi.org/10.1016/S0001-8686(97)00040-7.
[60] G. Narayanan, J. Shen, R. Boy, B.S. Gupta, A.E. Tonelli, Aliphatic polyester nanofibers functionalized with cyclodextrins and cyclodextrin-guest inclusion complexes, Polymers 10 (2018) 1–26, https://doi.org/10.3390/polym10040428.
[61] O. Laput, I. Vasenina, M.C. Salvadori, K. Savkin, D. Zuza, I. Kurzina, Low-temperature plasma treatment of polylactic acid and PLA/HA composite material, J. Mater. Sci. 54 (2019) 11726–11738, https://doi.org/10.1007/s10853-019-03693-4.
[62] E. Lih, S.H. Oh, Y.K. Joung, J.H. Lee, D.K. Han, Polymers for cell/tissue anti-adhesion, Prog. Polym. Sci. 44 (2015) 28–61, https://doi.org/10.1016/j.progpolymsci.2014.10.004.
[63] W. Limsukon, R. Auras, T. Smith, Effects of the three-phase crystallization behavior on the hydrolysis of amorphous and semicrystalline Poly(lactic acid)s, ACS Appl. Polym. Mater. 3 (2021) 5920–5931, https://doi.org/10.1021/acsapm.1c01080.
[64] L.S. Nair, C.T. Laurencin, Biodegradable polymers as biomaterials, Prog. Polym. Sci. 32 (2007) 762–798, https://doi.org/10.1016/j.progpolymsci.2007.05.017.
[65] I. Van Der Meulen, M. De Geus, H. Antheunis, R. Deumens, E.A.J. Joosten, C. E. Koning, A. Heise, Polymers from functional macrolactones as potential biomaterials: enzymatic ring opening polymerization, biodegradation, and biocompatibility, Biomacromolecules 9 (2008) 3404–3410, https://doi.org/10.1021/bm800898c.
[66] A.M. Rahimi, M. Cai, S. Hoyer-Fender, Heterogeneity of the NIH3T3 fibroblast cell line, Cells 11 (2022), https://doi.org/10.3390/cells11172677.